

## Article

# Nonlinear Performance Curve Estimation of Unreinforced Masonry Walls Subjected to In-Plane Rocking Behavior

Ho Choi <sup>1</sup>, Chunri Quan <sup>2</sup> and Kiwoong Jin <sup>3,\*</sup><sup>1</sup> Department of Architecture, Faculty of Science and Technology, Shizuoka Institute of Science and Technology, Fukuroi 4378555, Japan; choi.ho@sist.ac.jp<sup>2</sup> Department of Architecture, Graduate School and Faculty of Engineering, Osaka Institute of Technology, Osaka 5358585, Japan; chunri.quan@oit.ac.jp<sup>3</sup> Department of Architecture, School of Science and Technology, Meiji University, Kawasaki 2148571, Japan

\* Correspondence: jin@meiji.ac.jp; Tel.: +81-44-934-7338

**Abstract:** This study focused on the in-plane rocking behavior of unreinforced masonry (URM) walls. Three URM wall specimens were designed and fabricated based on a typical masonry house in Korea. The experimental parameters were the layout of openings (its presence or absence) and configuration of openings (window or door). Static cyclic loading tests were conducted to investigate nonlinear performance curves of masonry walls subjected to a rocking behavior in the in-plane direction. In this paper, the mortar-joint tensile crack strength and rocking strength of masonry walls (i.e., peak and residual strengths) were evaluated, and the effects of opening configurations on the masonry wall strength were examined, due to the proposed procedure. The deformation capacity of a rocking behavior was also identified by the procedure. As a result, specimens without initial cracks showed the rocking behavior after mortar-joint tensile crack failure, whereas a specimen with initial cracks exhibited only the rocking behavior. Since no remarkable strength deterioration was found until final loading in all specimens, an in-plane rocking URM wall may have very good deformation performance. The estimated mortar-joint tensile crack strength, rocking strength, stiffness, and ultimate deformation were in good agreement with the experimental results, regardless of the layout and configuration of openings.



**Citation:** Choi, H.; Quan, C.; Jin, K. Nonlinear Performance Curve Estimation of Unreinforced Masonry Walls Subjected to In-Plane Rocking Behavior. *Appl. Sci.* **2023**, *13*, 7298. <https://doi.org/10.3390/app13127298>

Academic Editors: José Neves and Asterios Bakolas

Received: 5 April 2023

Revised: 7 June 2023

Accepted: 16 June 2023

Published: 19 June 2023



**Copyright:** © 2023 by the authors. Licensee MDPI, Basel, Switzerland. This article is an open access article distributed under the terms and conditions of the Creative Commons Attribution (CC BY) license (<https://creativecommons.org/licenses/by/4.0/>).

## 1. Introduction

Unreinforced masonry (URM) buildings are the most representative construction system since the early ages of mankind. The increasing interest in this construction technique in the last few decades has resulted in many experimental tests on URM subassemblages [1–5] and on complete URM buildings [6–12]. These studies have provided significant valuable insights into the seismic performance of URM buildings. However, many characteristics of URM buildings are yet to be fully understood, and URM buildings are always severely damaged when an earthquake occurs [7,8,10–12].

On the other hand, most masonry buildings are less than three-story, and most of them are constructed without the consideration of earthquake design requirements or reference to any design code [13–18]. According to experimental studies on two-story masonry buildings conducted in the United States [4,19,20], URM walls exhibited a ductile behavior with a clear yield point and constant strength after yielding, even though no reinforcing bars were used. In the experimental studies by Kang et al. [21] and Yi et al. [22], deformation capacities of masonry walls with aspect ratio  $h/l$  ( $h$ : wall height,  $l$ : wall length) of 0.67 to 1.33 and 0.75 to 2.25 were found to be 2.0% to 5.0% and greater than 1.5 % of the lateral drift angle, respectively. Such ductile behavior of URM walls appears when the walls fail by rocking behavior or bed joint sliding behavior, from Figure 1 below. Based on these experimental results, in various seismic performance design guidelines [23–25],

deformation-dominant hysteresis models in nonlinear analysis are allowed for the rocking and bed joint sliding failures of URM walls.

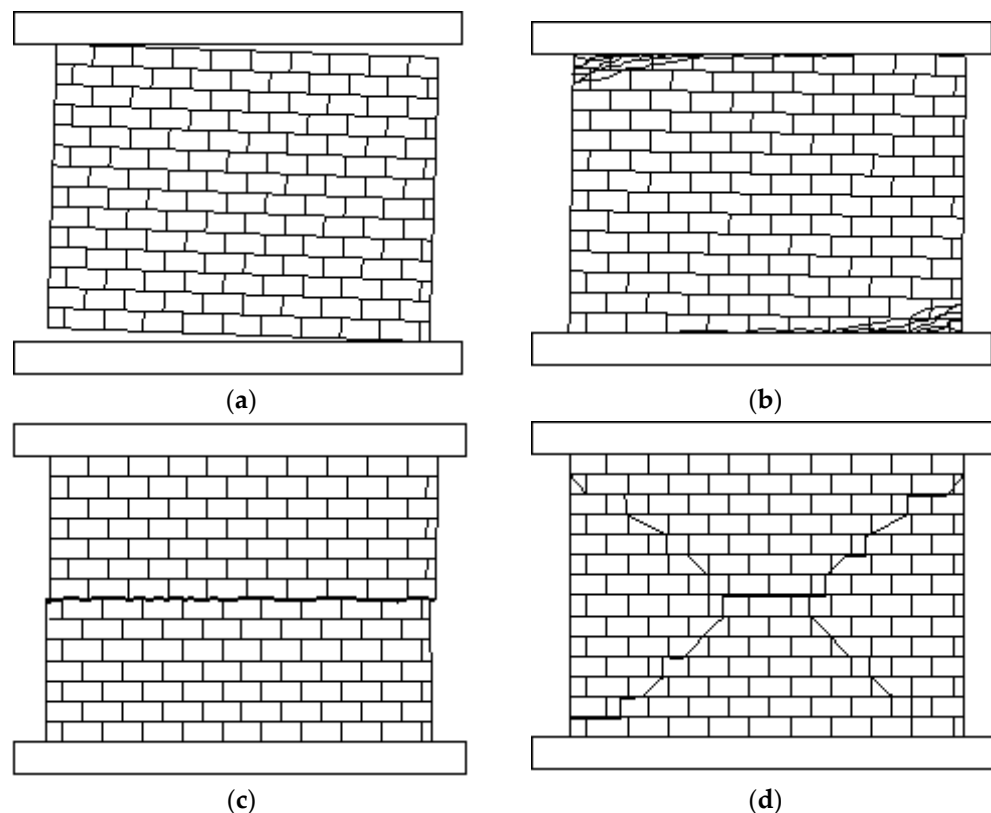


**Figure 1.** Representative failure modes of unreinforced masonry wall: (a) rocking failure mode; (b) toe crushing failure mode; (c) bed joint sliding failure mode; (d) diagonal tension failure mode.

The representative failure modes of URM walls resisting in-plane lateral loads are divided into four types, as shown in Figure 1: (a) rocking failure mode, (b) toe crushing failure mode, (c) bed joint sliding failure mode, and (d) diagonal tensile failure mode. The rocking failure mode and the bed joint sliding failure mode can be categorized as the ductile failure mode, as mentioned in the previous paragraph, whereas the toe crushing failure mode and the diagonal tensile failure mode can be categorized as the brittle failure mode [13,26–28]. The dominant failure mode of a URM wall depends on the aspect ratio of the wall, the material properties of the masonry unit and the joint mortar, and the axial load. According to the study by Eom et al. [29], since the axial load is generally not high in one- or two-story masonry buildings, the dominant failure mode of URM walls is mainly determined by the aspect ratio of the wall; the rocking failure or toe crushing failure are dominant at an aspect ratio greater than 1.8, and the bed joint sliding failure mode is dominant at an aspect ratio less than 1.8. In particular, the walls in low-rise masonry buildings have various openings such as doors and windows. Therefore, since the aspect ratios of most masonry walls with openings exceed 1.5, the walls in low-rise masonry buildings with openings mainly show the rocking failure or toe crushing failure. On the other hand, the toe crushing failure generally occurs at the compression end of walls after the rocking failure [19]. In addition, the toe crushing failure for a masonry wall with low axial load is defined as residual behavior after rocking failure in nonlinear analysis, according to ASCE 41-17 [25]. Therefore, it is important to understand the in-plane rocking behavior occurring in URM walls, and to quantitatively evaluate the strength, stiffness, and deformation capacity for the in-plane rocking behavior in order to reasonably assess the seismic performance of low-rise masonry buildings.

As mentioned above, the research on seismic performance evaluation of URM walls has made great progress. However, few studies have theoretically clarified the hysteresis characteristics of the rocking behavior, which is the main behavior of URM walls, e.g., [19–21,24–26,29]. Therefore, in this study, in-plane cyclic loading tests on the rocking behavior of URM walls were conducted, and a nonlinear performance curve evaluation procedure is suggested. In this test, three URM wall specimens were designed and fabricated based on a typical masonry house in Korea. The experimental parameters were the layout of openings (presence or absence) and the configuration of openings (window or door). Static cyclic loading tests were conducted to investigate nonlinear performance curves of masonry walls subjected to a rocking behavior in the in-plane direction. In this paper, the mortar-joint tensile crack strength and rocking strength of masonry walls (i.e., peak and residual strengths) were evaluated by the proposed procedure, the test results were compared, and the effects of opening configurations on the masonry wall strength were examined. The deformation capacity of a rocking behavior was also identified by the procedure.

This paper is organized as follows: Section 1 is the introduction; Section 2 is the experimental program, including reference building, test specimen, material characteristics, and test program; Section 3 is the experimental results, including failure patterns and the relationship between lateral load force and drift angle of each specimen; Section 4 is the evaluation of nonlinear performance curve subjected to in-plane rocking behavior, including mortar-joint tensile crack strength and nonlinear performance curve after mortar-joint cracking; and Section 5 is the conclusions.

## 2. Experimental Program

### 2.1. Reference Building

In this study, a typical masonry house in Korea was selected as the reference building because masonry buildings have been used in Korea for a long time. Figure 2 shows the outline of the reference building that has two stories with plan dimensions of 8.7 m by 8.7 m. The unreinforced masonry walls of the reference building consist of three layers: (1) red brick wall on the outside (0.5B length stacking,  $t = 100$  mm), (2) cement brick wall on the inside (0.5B length stacking,  $t = 100$  mm), and (3) insulation space (between the red and cement brick walls,  $t = 50$  mm).

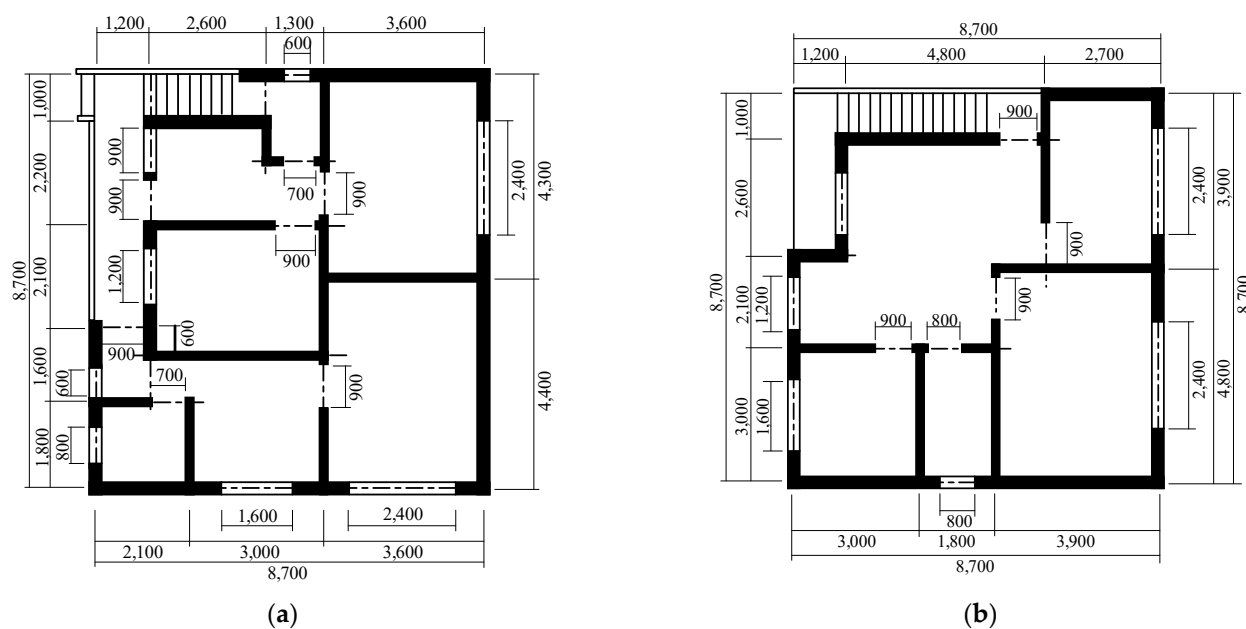


**Figure 2.** Outline of reference building: (a) first floor and (b) second floor (unit: mm).

## 2.2. Test Specimens

In this study, three full-scale, single-story specimens representing the first story of a two-story masonry house building were fabricated and tested under cyclic loading, as shown in Figure 3: (a) unreinforced masonry wall specimen without opening (Specimen M-N), (b) unreinforced masonry wall specimen with window opening (Specimen M-W), and (c) unreinforced masonry wall specimen with door opening (Specimen M-D). The specimen size is 1.97 m by 1.39 m, as shown in the figure. The sizes of the red brick and cement brick are  $210 \times 100 \times 60$  mm. Joint mortar with a thickness of 10 mm and a cement-to-sand ratio of 1:3.5, which is generally used in Korea, is placed horizontally and vertically between brick units in the walls. As shown in Figure 3, all specimens consisted of two layers with red brick and cement brick walls. In this study, the insulation space was disregarded because the insulation did not affect the shear force of the overall wall. The axial stress was calculated to be  $0.16 \text{ N/mm}^2$  for the first story of the reference building. The openings of the Specimens M-W and M-D were arranged asymmetrically to expect different failure patterns and different shear forces in positive and negative directions, as shown in Figure 3b,c. The opening ratio was set to 0.16 for the Specimens M-W and M-D based on previous research [21,22,29].

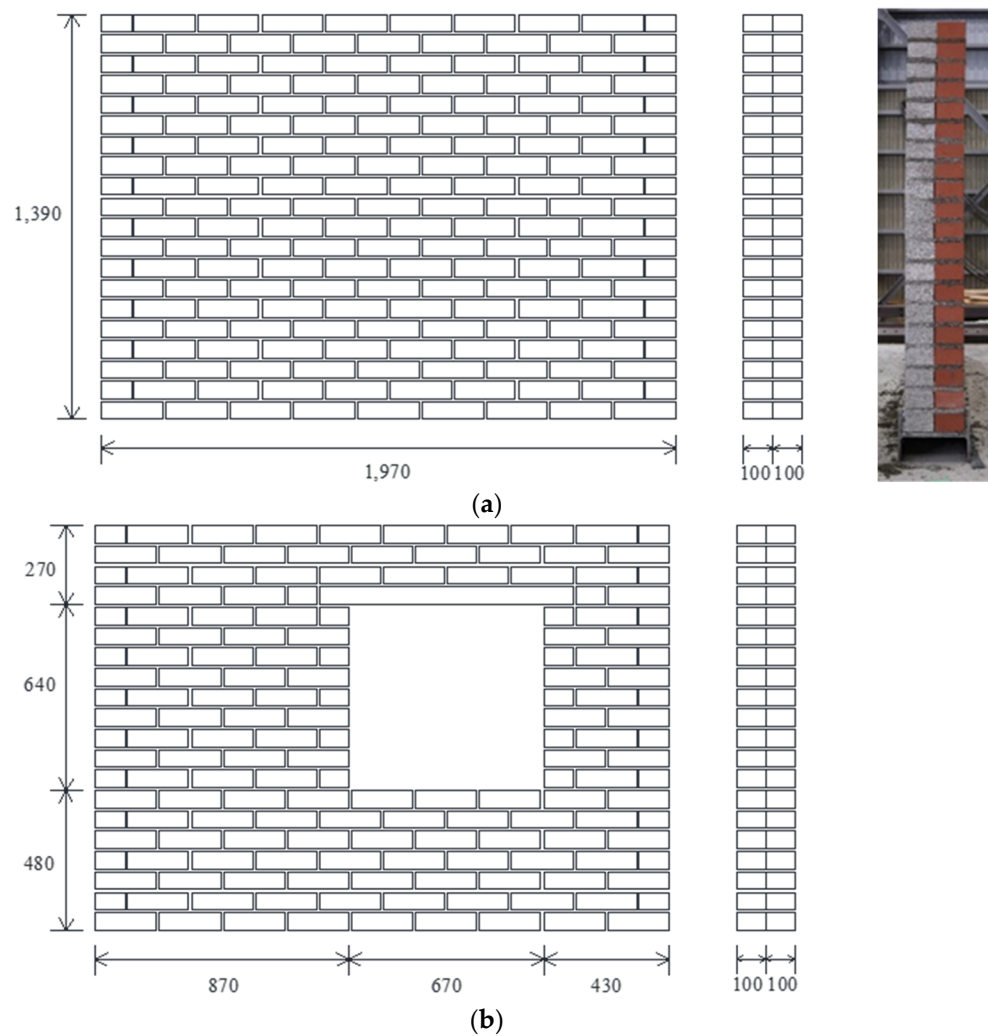


**Figure 3. Cont.**

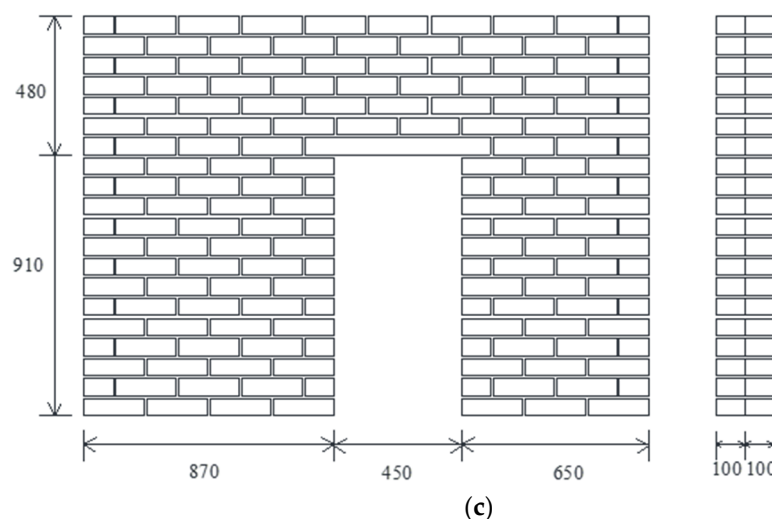


**Figure 3.** Elevations of the specimens: (a) Specimen M-N; (b) Specimen M-W; and (c) Specimen M-D (unit: mm).

### 2.3. Material Characteristics

The compressive strengths of each brick and joint mortar are shown in Table 1. As shown in the table, the compressive strength of the red brick was higher than that of the cement brick in both the single unit and 3-layered prism tests. In addition, the 3-layered prism compressive strengths of the cement and red bricks are about 43% and 41% of the single unit compressive strengths, respectively. The compressive strength of the joint mortar was considerably higher than those of the 3-layered prism of the masonry.

**Table 1.** Compressive strengths of each brick and joint mortar.

	Cement Brick		Red Brick		Joint Mortar <sup>(2)</sup> (N/mm <sup>2</sup> )
	Brick Unit (N/mm <sup>2</sup> )	Brick Prism <sup>(1)</sup> (N/mm <sup>2</sup> )	Brick Unit (N/mm <sup>2</sup> )	Brick Prism <sup>(1)</sup> (N/mm <sup>2</sup> )	
Test 1	37.3	15.7	46.4	18.4	39.5
Test 2	35.4	15.5	45.6	20.8	43.6
Test 3	35.3	15.4	45.6	16.7	52.1
Average	36.0	15.4	45.9	18.6	45.1

<sup>(1)</sup> 3-layered specimen, <sup>(2)</sup> cylinder type.

Some factors are needed to evaluate an in-plane rocking strength of URM masonry walls: an adhesive strength and a friction coefficient between the brick unit and mortar. Adhesive strengths  $\tau_0$  and friction coefficients  $\mu$  can be obtained from the relationship between shear stress  $\tau$  and axial stress  $\sigma_0$  based on the well-known Mohr's circle, as shown in Figure 4. As shown in Figure 4 and Equation (1), it is assumed that the shear stress and the axial stress are linearly related in the region where the axial stress is not high (the hatched part); hence, the slope and  $y$ -intercept are the friction coefficient  $\mu$  and adhesive strength  $\tau_0$ , respectively [30]. In this study, the bed joint sliding tests were conducted using the 3-layered prism specimens to investigate the adhesive force and friction coefficient. Figure 5 shows the test overview. In this test, the experimental parameter is the axial stress  $\sigma_0$  of 0.3, 0.5, and 0.7 N/mm<sup>2</sup>; the axial force corresponding to the axial stress was applied with four steel bars, as shown in Figure 5. The target axial force was confirmed by the value measured from the strain gauges attached to each steel bar. The strain value for each axial force was calculated using Equations (2) and (3). The Young's modulus of the steel bar was obtained from an additional tensile test.

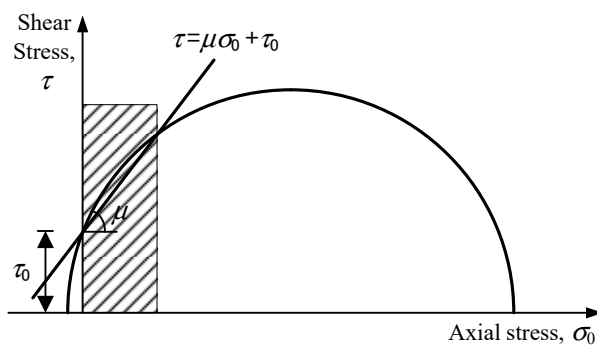


**Figure 4.** Shear stress and axial stress relationships based on Mohr's circle.

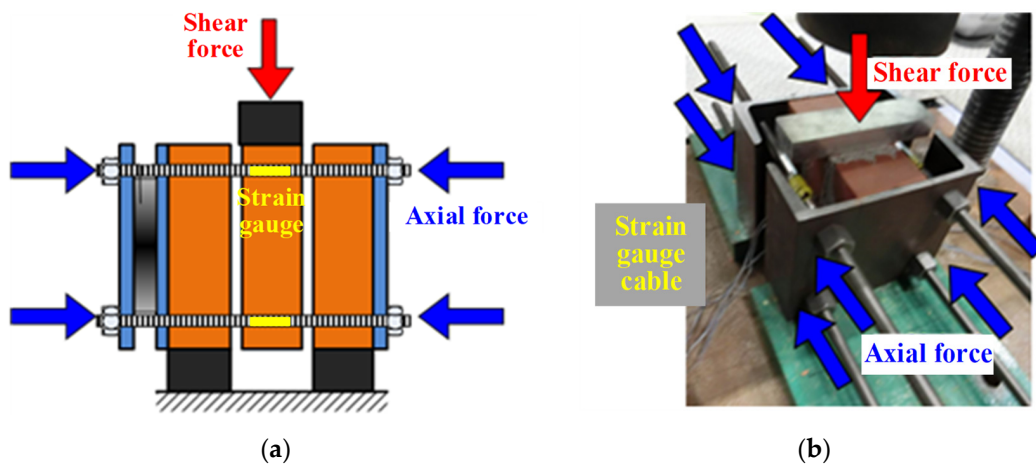


**Figure 5.** Bed joint sliding test using 3-layered prism specimen: (a) schematic of the test and (b) test setup.

Table 2 and Figure 6 show the test results and the relationship between the shear stress and the axial stress, respectively. Consequently, the friction coefficient and adhesive strength of the cement and red bricks were obtained from the linear regression analysis on the experimental data, as shown in Figure 6. As shown in the figure, it was found that the friction coefficient and adhesive strength of the cement and red bricks were almost the same.

$$\tau = \mu \cdot \sigma_0 + \tau_0 \quad (1)$$

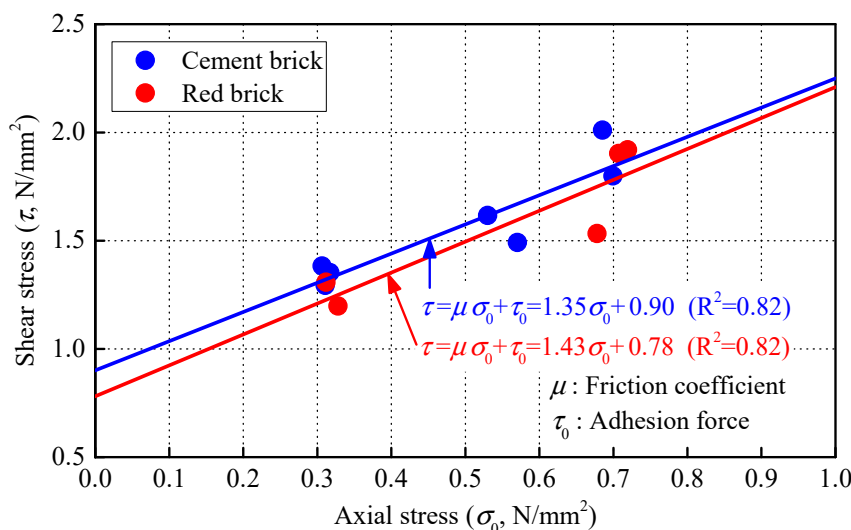
where

**Table 2.** The results of bed joint sliding failure tests.

Brick Type	Target Axial Stress, $\sigma_0$ (N/mm <sup>2</sup> )	Target Strain, $\varepsilon$ ( $\mu$ /bar)	Specimen No.	Achieved Axial Stress, $\sigma$ (N/mm <sup>2</sup> )	Maximum Shear Stress, $\tau$ (N/mm <sup>2</sup> )
Cement brick	0.3	34.5	Test 1	0.31	1.29
			Test 2	0.32	1.35
			Test 3	0.31	1.38
	0.5	57.5	Test 1	0.57	1.49
			Test 2	0.53	1.62
	0.7	80.5	Test 1	0.70	1.80
			Test 2	0.69	2.01

**Table 2.** Cont.

Brick Type	Target Axial Stress, $\sigma_0$ (N/mm <sup>2</sup> )	Target Strain, $\varepsilon$ ( $\mu$ /bar)	Specimen No.	Achieved Axial Stress, $\sigma$ (N/mm <sup>2</sup> )	Maximum Shear Stress, $\tau$ (N/mm <sup>2</sup> )
Red brick	0.3	34.5	Test 1	0.33	1.20
			Test 2	0.31	1.31
			Test 1	0.68	1.53
	0.7	80.5	Test 2	0.72	1.92
			Test 3	0.71	1.90

**Figure 6.** Shear stress and axial stress relationship under bed joint sliding failure.

$\tau$ : Shear stress under bed joint sliding failure (N/mm<sup>2</sup>);

$\mu$ : Friction coefficient (1.35 and 1.43 in cement and red bricks, respectively);

$\sigma_0$ : Target axial stress (N/mm<sup>2</sup>);

$\tau_0$ : Adhesive strength (N/mm<sup>2</sup>, 0.90 and 0.78 in cement and red bricks, respectively).

$$N' = \frac{\sigma_0 \times A_b}{4} \quad (2)$$

$$\varepsilon = \frac{N'}{E_s \times A_s} \quad (3)$$

where

$N'$ : Target axial force per steel bar (N);

$\sigma_0$ : Total target axial stress (0.3, 0.5 and 0.7 N/mm<sup>2</sup>, herein);

$A_b$ : Cross-sectional area of two sides of brick (=2 × 210 × 100 mm<sup>2</sup>);

$\varepsilon$ : Target strain value per steel bar;

$E_s$ : Young's modulus of steel bar (=2.01 × 10<sup>5</sup> N/mm<sup>2</sup>);

$A_s$ : Nominal cross-sectional area of steel bar ( $\phi 17 = 227$  mm<sup>2</sup>).

#### 2.4. Test Program

A loading system for the in-plane static cyclic tests is shown in Figure 7. Lateral loads in the positive and negative directions were applied to the left end of the upper beam with hydraulic actuators. A vertical hydraulic actuator was installed to apply a constant axial load of 62 kN (0.16 N/mm<sup>2</sup>) on the upper beam. Figure 8 shows a lateral loading protocol that was controlled by a drift angle  $R$ , defined as a lateral drift  $\Delta$  at the top-center of the

specimen divided by the height from the bottom of the specimen,  $H$ , as shown in Figure 7. As shown in Figure 8, the peak drift angles of 0.1, 0.2, 0.4, 0.67, 1.0, 1.5, 2.0, 3.0, 4.0 and 5.0% are planned, and 2 cycles for each peak drift are imposed. After severe damage is found, the specimen is pushed over to collapse.

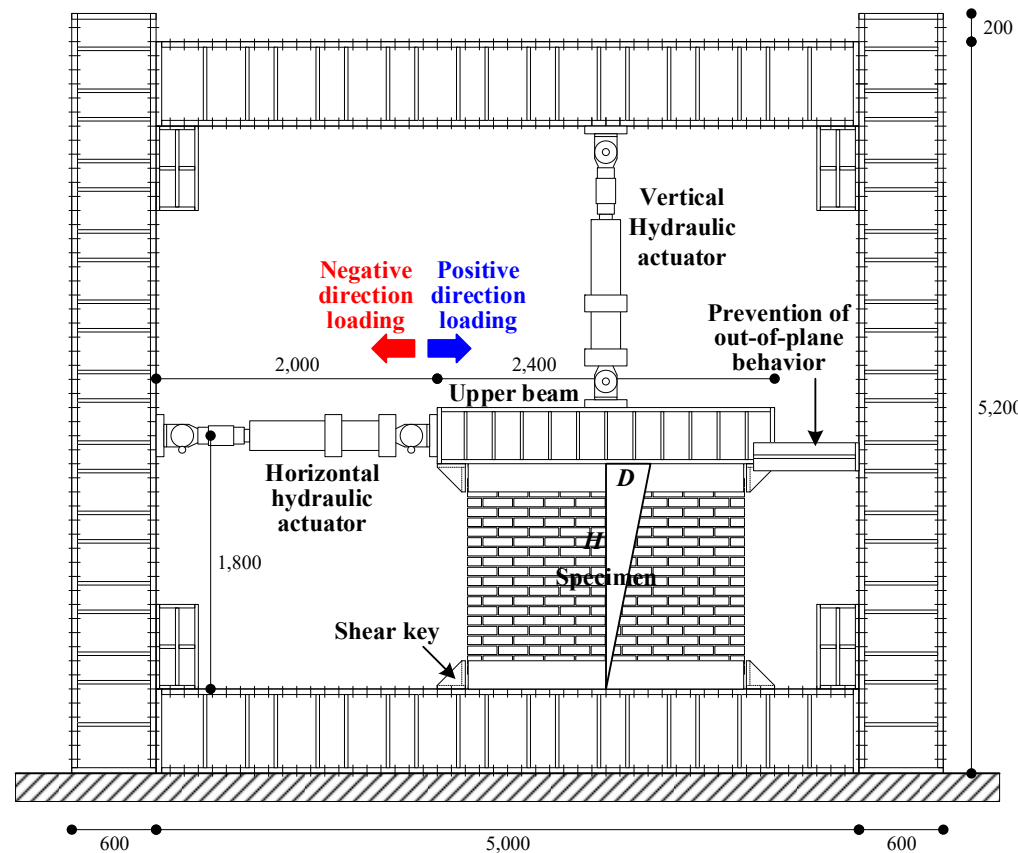


**Figure 7.** Loading system (unit: mm).

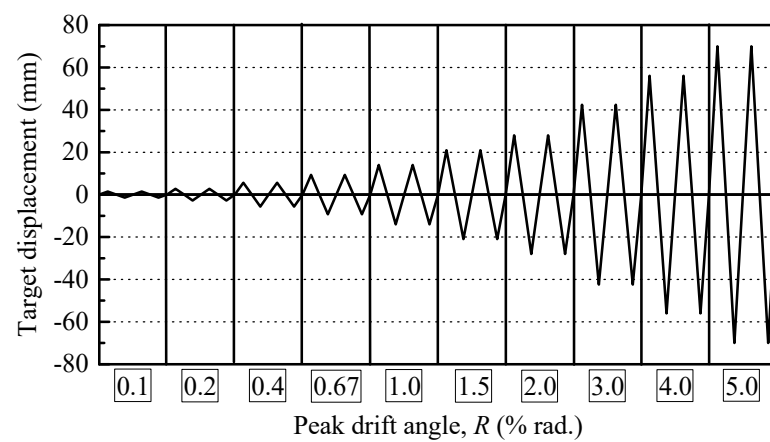


**Figure 8.** Lateral loading protocol.

The measurement system is shown in Figure 9. The relative lateral displacement, the lateral displacement at up and down opening of the wall, and the vertical displacement of both ends of the specimen were measured. Furthermore, the maximum crack widths at peak loads, and residual crack widths at unloaded stages were carefully measured.

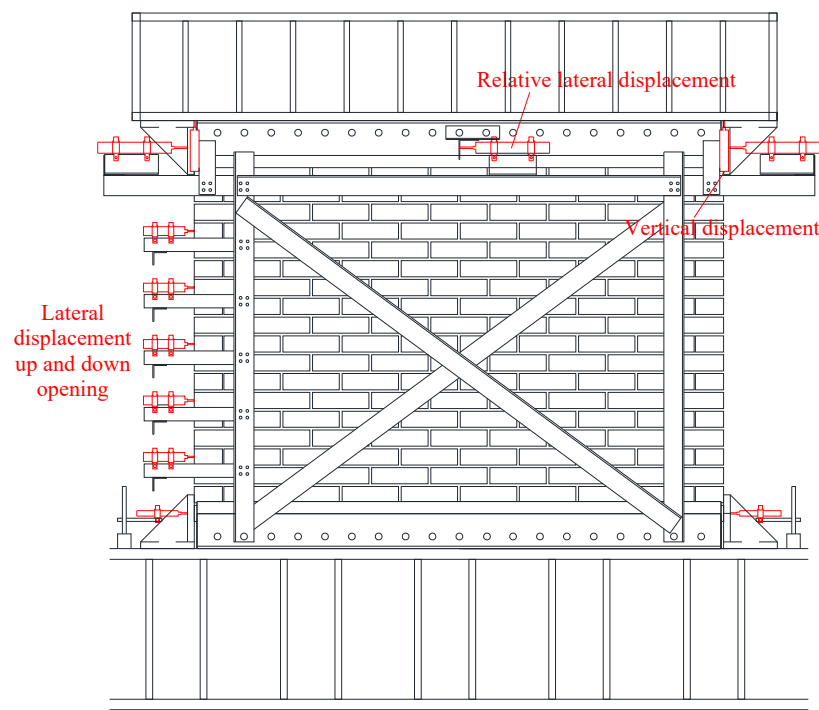
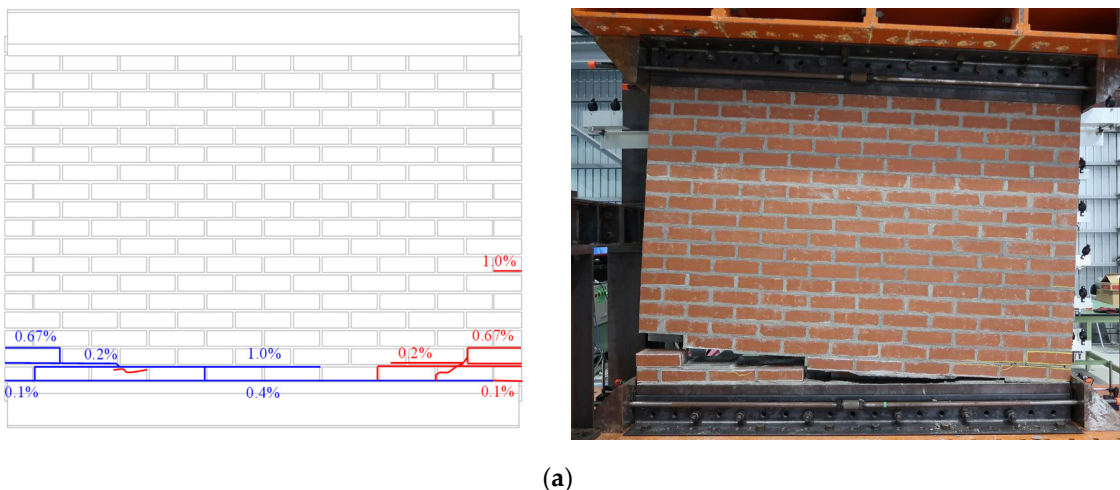


**Figure 9.** Measurement system (backside of the specimen).

### 3. Experimental Results: Failure Patterns and Lateral Force–Drift Angle Relationships

Figures 10 and 11 show the damage patterns after final loading and the lateral force–drift angle relationships of all specimens, respectively. The behavior of each specimen to failure is summarized below.



(a)

**Figure 10. Cont.**

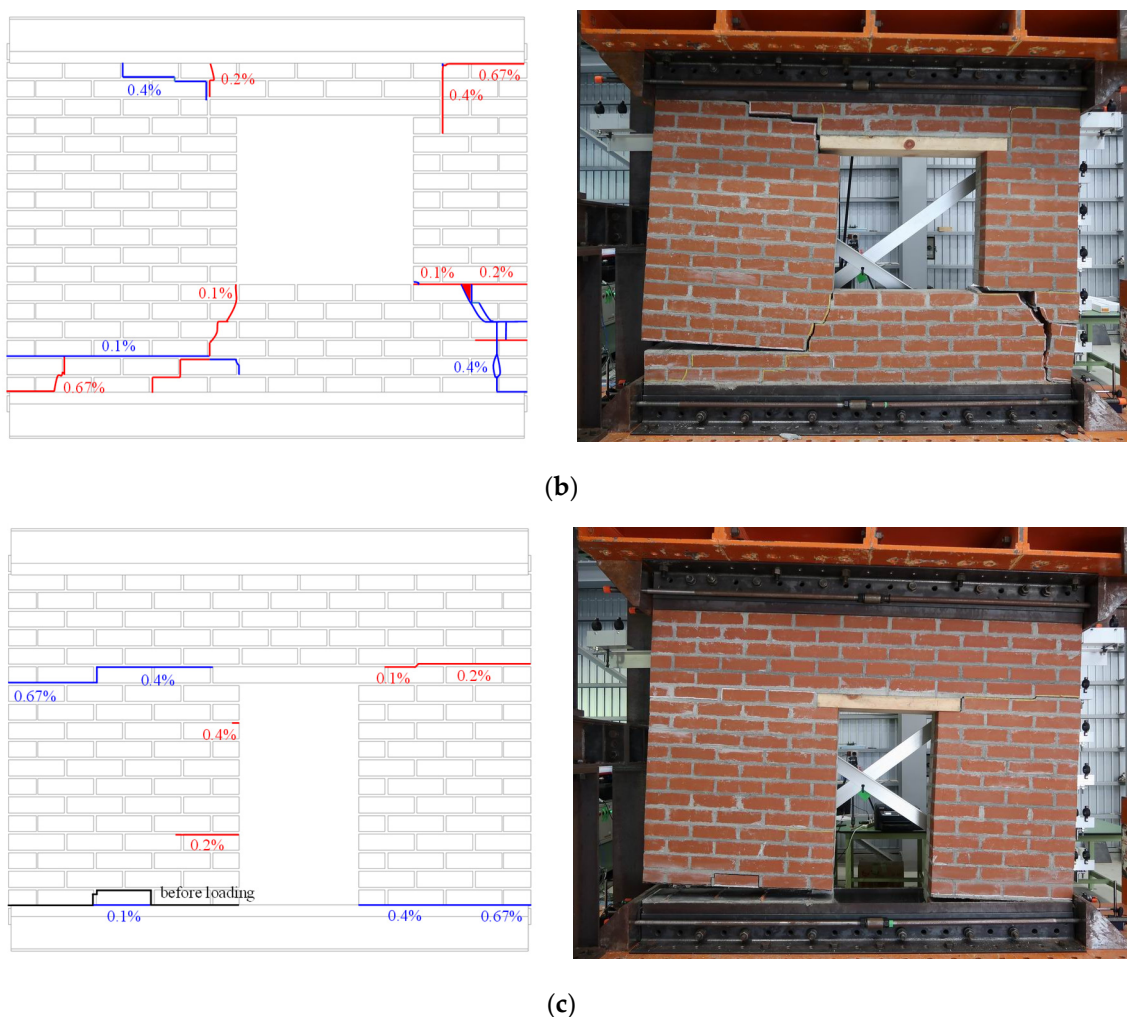


**Figure 10.** Final crack patterns (blue line: positive direction loading, red line: negative direction loading, black line: initial cracks): (a) Specimen M-N; (b) Specimen M-W; (c) Specimen M-D.

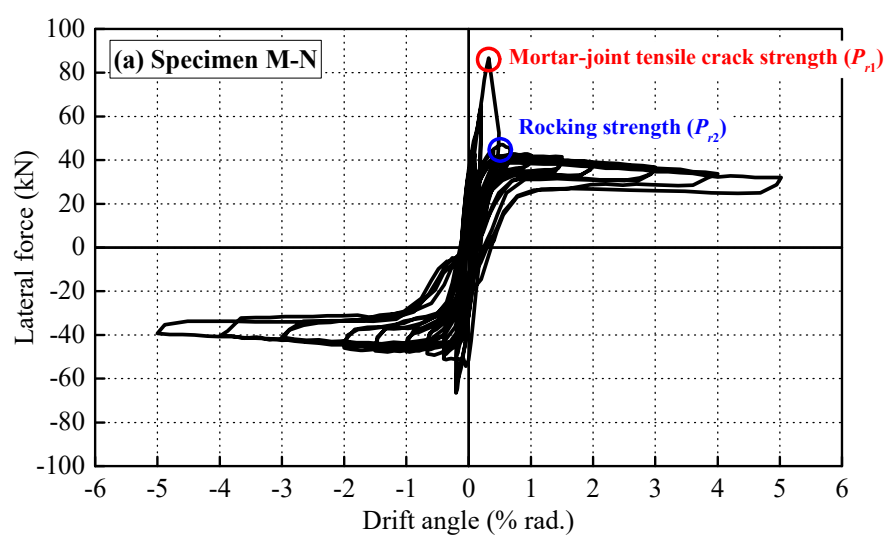


**Figure 11.** Cont.

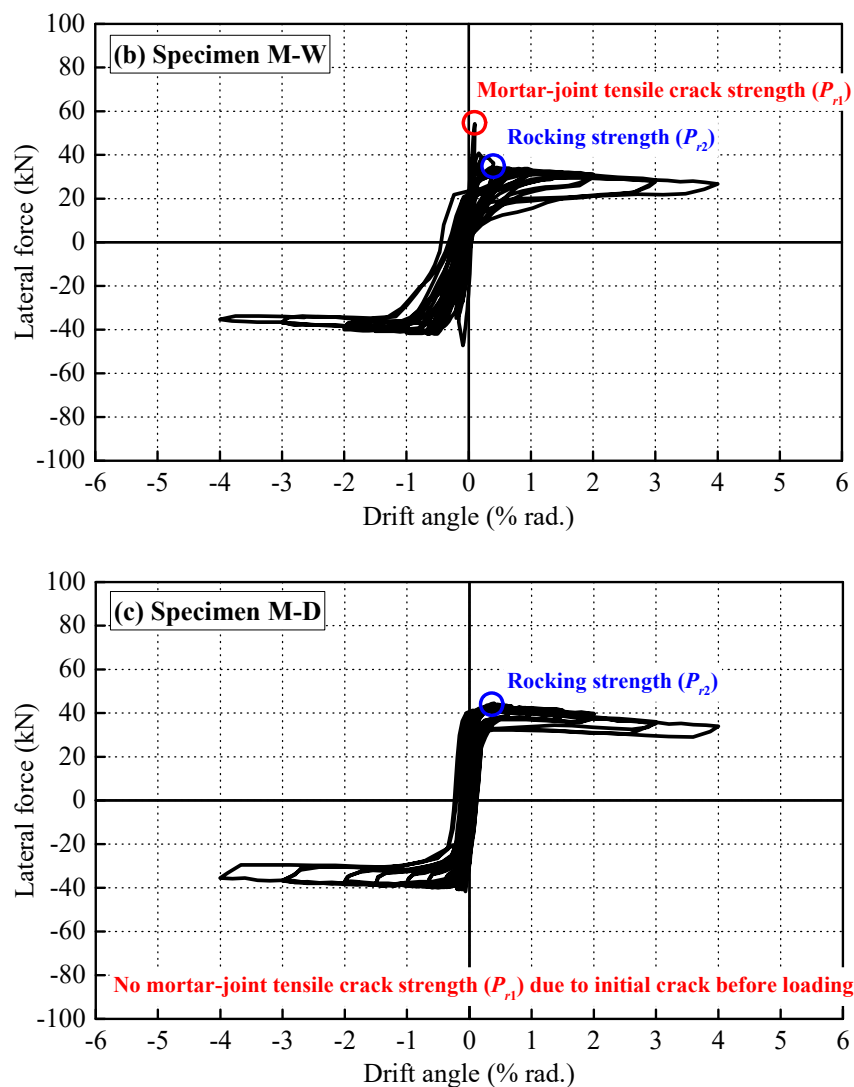


**Figure 11.** Lateral force–drift angle relationships of each specimen: (a) Specimen M-N; (b) Specimen M-W; (c) Specimen M-D.

### 3.1. Specimen M-N

During the first loading drift,  $R$ , of 0.1% rad., cracks were observed in the second bed joint. At  $R = 0.4\%$  rad., the cracks were newly found in the first and third bed joints, and the crack in the second bed joint developed over the entire length of the wall, causing the mortar-joint tensile crack failure. After  $R = 0.4\%$  rad., the rocking behavior was observed due to the entire bed joint crack. The maximum strength—the mortar-joint tensile crack strength  $P_{r1}$ —of 86.8 kN was recorded at  $R = 0.4\%$  rad., and then the strength rapidly deteriorated to 47.0 kN—the rocking strength  $P_{r2}$ —due to the mortar-joint tensile crack failure. From the  $R = 0.67\%$  showing the rocking behavior, no remarkable strength deterioration was found until final loading.

### 3.2. Specimen M-W

At the first loading drift,  $R = 0.1\%$  rad., the stair-stepped crack and bed joint crack were observed in the left and right sides of the window opening, respectively. At  $R = 0.2\%$  rad., the bed joint crack developed over the entire length of the wall, causing the mortar-joint tensile crack failure. After  $R = 0.2\%$  rad., the rocking behavior was observed due to the entire bed joint crack. The maximum strength of 54.3 kN ( $P_{r1}$ ) was recorded at  $R = 0.1\%$  rad., and then the strength rapidly deteriorated to 41.8 kN ( $P_{r2}$ ) due to the bed joint

sliding failure. From the  $R = 0.4\%$  showing the rocking behavior, no remarkable strength deterioration is found until final loading.

### 3.3. Specimen M-D

In this specimen, since the initial crack occurred in the lower left side along about 70% of the whole length of the wall, including the opening before loading, the strength due to the mortar-joint tensile crack failure did not appear clearly. The maximum strength of 44.0 kN ( $P_{r2}$ ) was recorded at  $R = 0.4\%$  rad. After  $R = 0.4\%$  rad., entire bed joint cracks were observed around the door opening. There was no remarkable strength deterioration until final loading.

## 4. Evaluation of Nonlinear Performance Curve Subjected to In-Plane Rocking Behavior

### 4.1. Strengths Subjected to In-Plane Rocking Behavior

The low-rise masonry buildings with strong mortar adhesion and/or no openings show the rocking behavior after tensile cracks occur at joint mortar, as shown in Figure 12a. On the other hand, low-rise masonry buildings with weak mortar adhesion, large opening ratio, and/or initial crack show only the rocking behavior, as shown in Figure 12b. As shown in Figure 11, Specimen M-N without opening showed both tensile crack generation and the rocking behavior. Specimen M-W with window opening and no initial crack also showed tensile crack generation, but the peak strength is not clear compared to Specimen M-N. In contrast, Specimen M-D with door opening and initial crack did not show tensile crack generation.

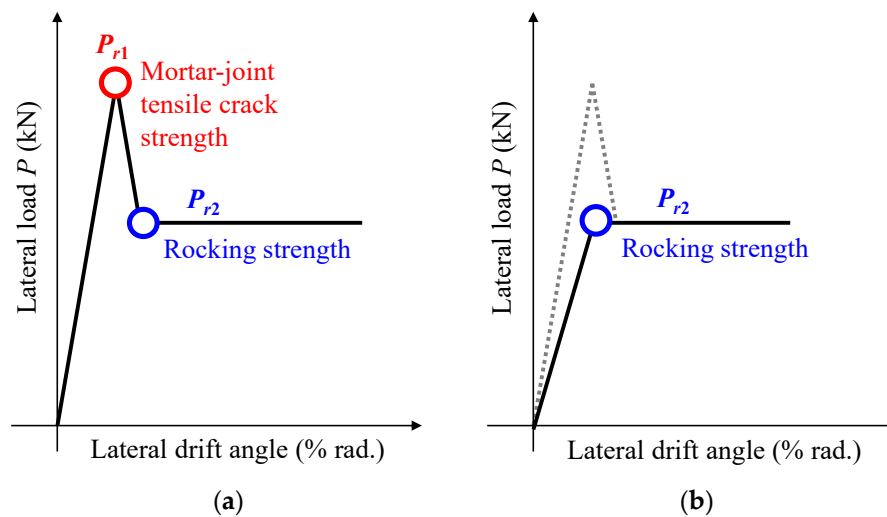


**Figure 12.** Idealized force–deformation relationship of in-plane rocking behavior in masonry walls: (a) with peak and (b) without peak.

### 4.2. Evaluation of Mortar-Joint Tensile Crack Strength

Figure 13 shows the relationship between the mortar-joint tensile crack strength  $P_{r1}$  (shown in Figure 12a), axial force, and stress distribution of solid masonry walls subjected to rocking behavior. In this study, it was assumed that the stress distribution before mortar-joint tensile failure is linear, and the peak strength occurs when the maximum tensile stress reaches the mortar-joint tensile strength  $f_{bjt}$  [31]. Since the flexural moment and axial force acting on the bottom of a wall are  $P_{r1} H$  and  $(N_D + W)$ , respectively, Equation (4) must be satisfied at the peak strength. From Equation (4), the mortar-joint tensile crack strength  $P_{r1}$  is determined by Equation (5). The  $P_{r1}$  of the perforated masonry walls is determined by considering the reduction factor  $\gamma$  in the  $P_{r1}$  of the solid masonry walls, as shown in Equation (6). Since the mortar-joint tensile failure mainly occurs in the bed joints, it is assumed that the factor  $\gamma$  is the ratio of wall length excluding opening length to whole wall length;  $\gamma = 0.66$  and 0.77 in Specimens M-W and M-D, respectively. The

estimated results of the mortar-joint tensile crack strength in each specimen, based on the above-described procedure, are shown in Table 3 and Figure 17 plotted as red lines, compared to the test results. In Specimens M-N and M-W, where mortar-joint tensile failure occurred, the estimated results show good agreement with the experimental results.

$$\frac{P_{r1} \cdot H}{(l^2 \cdot t) / 6} - \frac{N_D + W}{l \cdot t} = f_{bjt} \quad (4)$$

$$P_{r1} = \left( f_{bjt} + \frac{N_D + W}{l \cdot t} \right) \frac{l^2 \cdot t}{6H} \quad (5)$$

$$P_{r1} = \gamma \left( f_{bjt} + \frac{N_D + W}{l \cdot t} \right) \frac{l^2 \cdot t}{6H} \quad (6)$$

where

$P_{r1}$ : Mortar-joint tensile crack strength (kN);

$H$ : Height from the bottom of the wall to the loading point (=1800 mm, herein);

$h$ : Wall height (=1390 mm, herein);

$l$ : Wall length (=1970 mm, herein);

$t$ : Wall thickness (=200 mm, herein);

$N_D$ : Applied axial force (=62 kN);

$W$ : Wall self-weight (=10.43, 8.8, and 8.8 kN in Specimens M-N, M-W, and M-D, respectively);

$f_{bjt}$ : Maximum tensile stress of joint mortar (=0.84 N/mm<sup>2</sup> of average adhesive strength in cement and red bricks shown in Figure 5);

$\gamma$ : Reduction factor (the ratio of wall length excluding opening length to whole wall length, 0.66 and 0.77 in Specimens M-W and M-D, respectively).

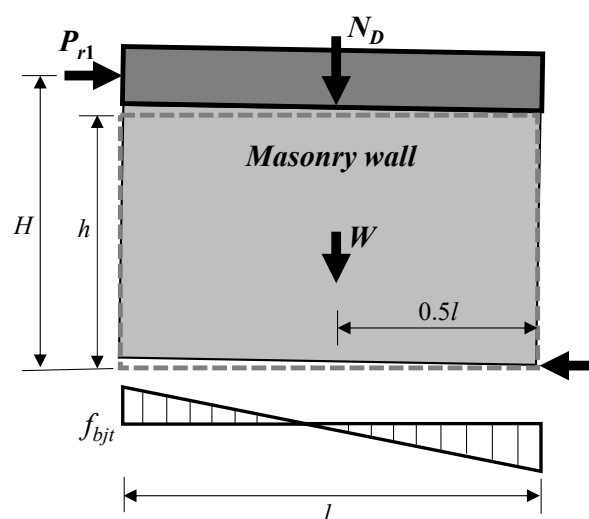


**Figure 13.** The relationship between mortar-joint tensile crack strength, axial force, and stress distribution of a solid masonry wall showing rocking behavior.

**Table 3.** Estimated and experimental results of the mortar-joint tensile crack strength.

	Specimen M-N	Specimen M-W	Specimen M-D
Experimental result	86.8 kN	54.3 kN	–
Estimated result	81.9 kN	53.8 kN	62.9 kN
Estimated/Experimental	0.94	0.99	–

#### 4.3. Evaluation of Nonlinear Performance Curve after Mortar-Joint Cracking

Figure 14 shows the relationship between the rocking strength  $P_{r2}$  (shown in Figure 12a,b), axial force, and stress distribution of solid masonry wall subjected to rocking behavior. After mortar-joint tensile failure, the stress exists only at the compression end with length  $a$ , as shown in Figure 14. In this study, the rocking strength  $P_{r2}$  was calculated assuming a uniformly distributed average stress  $0.8f_m'$  (i.e., 80% of the compressive strength of the masonry prism). Since the flexural moment and axial force acting on the bottom of a wall are  $P_{r2}H$  and  $(N_D + W)$ , respectively, Equation (7) must be satisfied at the rocking strength. From Equation (7), the rocking strength  $P_{r2}$  is determined by Equation (8).

$$P_{r2} \cdot H = (N_D + W)(0.5l + 0.5a) \quad (7)$$

$$P_{r2} = (N_D + W) \left( \frac{l}{2H} \right) \left( 1 - \frac{N_D + W}{0.8f_m' \cdot l \cdot t} \right) \quad (8)$$

where

$P_{r2}$ : Rocking strength (kN);

$a$ : Length of uniformly distributed stress block;

$f_m'$ : Compressive strength of masonry prism ( $=15.4 \text{ N/mm}^2$ , the lowest value in cement and red bricks shown in Table 1).

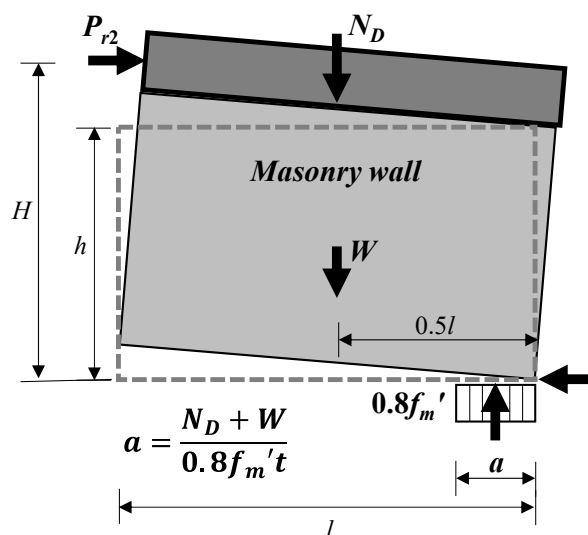


**Figure 14.** The relationship between rocking strength, axial force, and stress distribution of solid a masonry wall after mortar-joint cracking.

On the other hand, in the perforated masonry walls after mortar-joint cracking, the left and right walls of an opening individually rotate, as shown in Figure 15. Therefore, in this study, the rocking strength of perforated masonry walls after mortar-joint cracking is obtained as the sum of the strengths of each wall divided by openings, as shown in Figure 15a. Each rocking strength  $P_{r2}'$  can be calculated from the moment equilibrium condition, as shown in Equation (9). Since the self-weight of an individual wall is very small compared to an applied axial force, it can be set as  $N_D' \approx N_D' + W'$ . Therefore, the rocking strength of an individual wall in Equation (9) can be simplified as in Equation (10). Furthermore, the effective height  $h_e$  shown in Figure 15b was used for the height of individual walls according to ASCE 41-17 [25]. The prime symbols in Figure 15 and Equations (9) and (10) mean each parameter of an individual wall.

$$P_{r2}' = N'_D \left( \frac{l'}{2h'} \right) \left( 1 - \frac{N'_D}{0.8f'_m \cdot l' \cdot t} \right) + (N'_D + W') \left( \frac{l'}{2h'} \right) \left( 1 - \frac{N'_D + W'}{0.8f'_m \cdot l' \cdot t} \right) \quad (9)$$

$$P'_{r2} = (N'_D + W') \left( \frac{l'}{h_e} \right) \left( 1 - \frac{N'_D + W'}{0.8f_m \cdot l' \cdot t} \right) \quad (10)$$

where

$h_e$ : Effective wall height (mm).

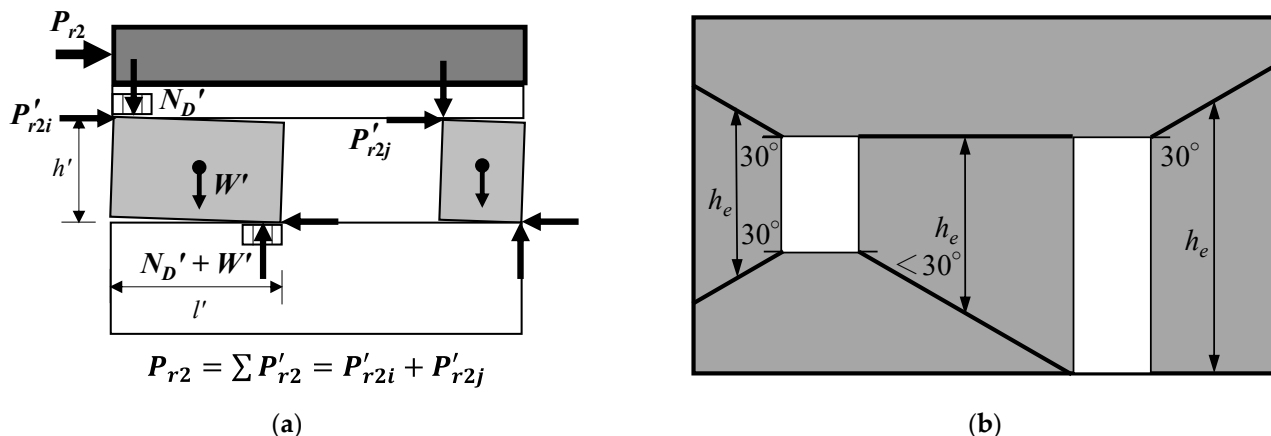


**Figure 15.** The relationship between rocking strength, axial force, and stress distribution of a perforated masonry wall after mortar-joint cracking: (a) rocking strength and (b) effective wall height.

The lateral behavior of an URM wall subjected to a rocking mechanism can be modeled with a nonlinear flexural and shear hinge, as shown in Figure 16a. In addition, each wall performance curve was replaced by a trilinear function with yielding and toe crushing points, as shown in Figure 16b [19,25]. According to this performance curve, the ultimate deformation  $\Delta_{tc,r}$  of the rocking behavior of URM walls is determined by toe crushing. The elastic stiffness  $k$  of an URM wall subjected to the rocking behavior in Figure 16a can be calculated by Equation (11), assuming that the flexural and shear springs are connected in series.

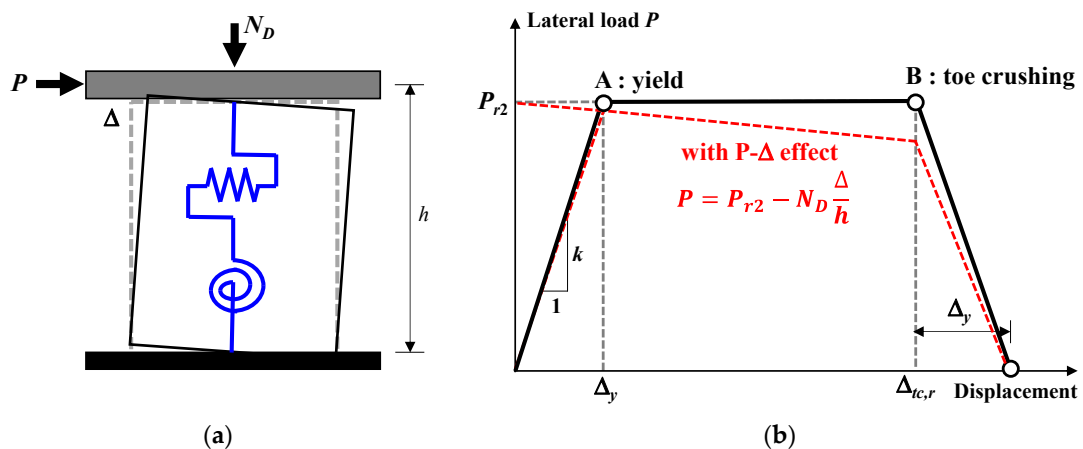


**Figure 16.** Modeling of URM walls subjected to rocking behavior: (a) flexural and shear hinge model of URM walls and (b) nonlinear performance curve.

The ultimate deformation  $\Delta_{tc,r}$  at the toe crushing failure can be calculated by integrating the curvature  $\phi_{tc,r}$  along wall height [19,25]. The curvature  $\phi_{tc,r}$  is calculated by dividing the strain by the length of the compressive side, as shown in Equation (12), and the ultimate deformation  $\Delta_{tc,r}$  is finally obtained by integrating the curvature twice, as shown in Equation (13).

$$k = \frac{1}{\frac{h^3}{\alpha \cdot E_m \cdot I_{gm}} + \frac{h}{G_m \cdot A_m}} \quad (11)$$

$$\phi_{tc,r} = \frac{\varepsilon_{mu}}{c} = \frac{\varepsilon_{mu}}{a/0.8} \quad (12)$$

$$\Delta_{tc,r} = \beta \cdot \phi_{tc,r} \cdot h^2 \quad (13)$$

where

$k$ : Elastic stiffness (N·mm);

$\alpha$ : 3 for a cantilever wall and 12 for a fixed-fixed wall (=3, herein);

$E_m$ : Masonry elastic modulus ( $=1810$  N/mm $^2$  from the results measured using displacement transducers between first and third layers during the 3-layered prism tests, herein);

$I_{gm}$ : Moment of inertia for the gross section of the wall;

$G_m$ : Masonry shear modulus ( $=0.4E_m$ , herein);

$A_m$ : Cross-sectional area of the wall;

$\phi_{tc,r}$ : Curvature at toe crushing failure;

$\varepsilon_{mu}$ : Strain at toe crushing failure ( $=0.0035$ , herein);

$c$ : Depth to neutral axis;

$a$ : Length of uniformly distributed stress block in Figure 14;

$\Delta_{tc,r}$ : Ultimate deformation;

$\beta$ : Coefficient depending on the dominant behavior mode, 1/3 for single curvature and 1/4 for double curvature (1/3 for Specimen M-N, 1/4 for Specimens M-W and M-D, herein).

The estimated nonlinear performance values subjected to the rocking behavior are shown in Table 4, and the nonlinear performance curves are shown in Figure 17, respectively, compared to the test results. For all specimens, not only the estimated rocking strengths, but also the overall nonlinear performance curves based on the proposed procedure, were in good agreement with the experimental results, regardless of the presence or absence of an opening.

**Table 4.** Nonlinear performance values subjected to the rocking behavior shown in Figure 16b.

	Specimen M-N	Specimen M-W	Specimen M-D
Rocking strength $P_{r2}$ (kN)	43.7 (47.0)	42.2 (41.8)	42.8 (44.0)
Elastic stiffness $k$ (N/mm)	$8.46 \times 10^4$	$7.10 \times 10^4$	$7.10 \times 10^4$
Yielding deformation $\Delta_y$ (mm)	0.52	0.59	0.60
Toe crushing strength $P$ (kN)	40.6	40.8	40.6
Ultimate deformation $\Delta_{tc,r}$ (mm)	91.2	57.8	68.1

( ): Test results.

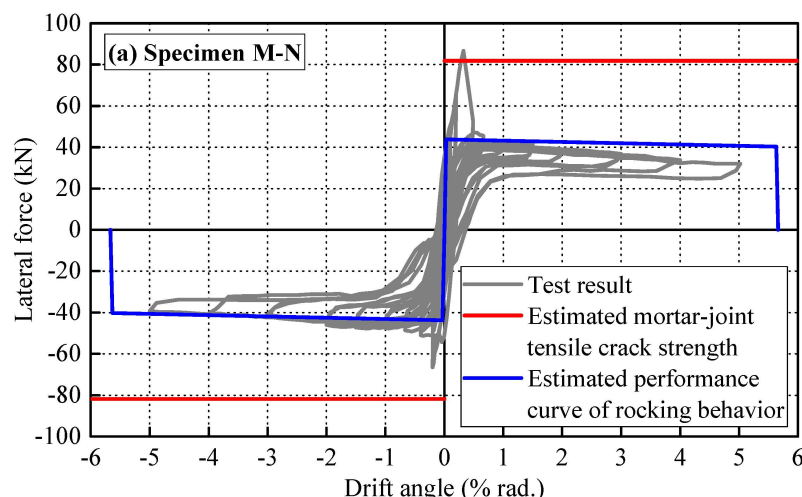


**Figure 17.** Cont.

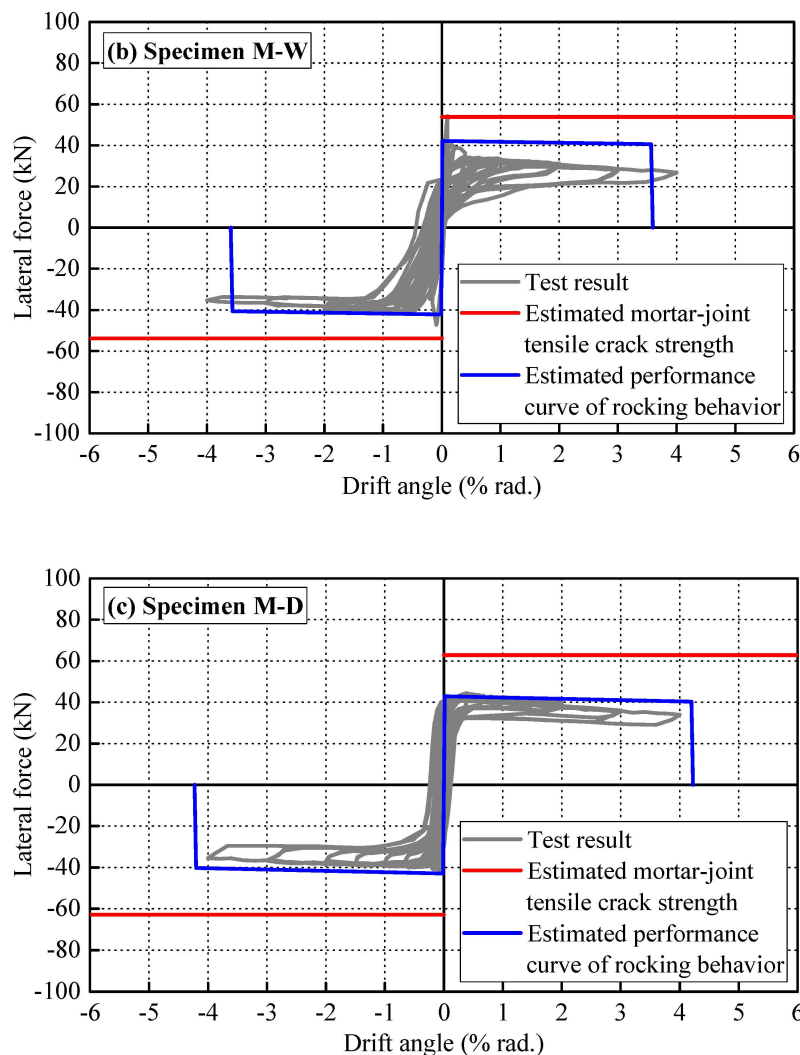


**Figure 17.** Estimated and measured load-deformation relations of each specimen: (a) Specimen M-N; (b) Specimen M-W; (c) Specimen M-D.

Using the proposed procedure in this study, it is possible to estimate the nonlinear performance curve of the rocking behavior, including the ultimate deformation level, as well as the mortar-joint tensile crack strength of solid and perforated rocking URM walls.

## 5. Conclusions

The current paper presents the experimental tests of one solid and two perforated unreinforced masonry walls subjected to the rocking behavior, and investigated peak and residual strengths, deformation capacity, and hysteresis characteristics. The following major findings were obtained:

1. Specimens M-N and M-W without an initial crack showed the rocking behavior after mortar-joint tensile crack failure, whereas Specimen M-D with an initial crack showed only the rocking behavior. For all specimens, no remarkable strength deterioration was found until final loading.
2. The mortar-joint tensile crack strengths of each specimen were estimated based on the maximum tensile stress of joint mortar. In Specimens M-N and M-W, where the mortar-joint tensile failure occurred, the estimated results based on the proposed procedure show good agreement with the experimental results.
3. The rocking strengths and the nonlinear performance curves of each specimen were estimated based on the length of the compressive side, the compressive strength of

the masonry prism, and openings. For all specimens, not only the estimated rocking strengths, but also the nonlinear performance curves based on the proposed procedure, were in good agreement with the experimental results, regardless of the presence or absence of an opening.

4. Using the proposed procedure in this study, it is possible to estimate the hysteresis characteristics of the rocking behavior, including the ultimate deformation level, as well as the mortar-joint tensile crack strength of solid and perforated rocking URM walls.

The current paper focused only on the in-plane rocking behavior of URM walls. In future studies, the out-of-plane behavior of URM walls should be investigated experimentally and theoretically. Furthermore, the proposed analytical procedure should be applied to other experimental results to verify the accuracy of this procedure.

**Author Contributions:** All authors have contributed to the development of the research and in the elaboration of this article. C.Q. and K.J. contributed to the methodology and experimental research, and edited the manuscript. All authors have read and agreed to the published version of the manuscript.

**Funding:** This research received no external funding.

**Institutional Review Board Statement:** Not applicable.

**Informed Consent Statement:** Not applicable.

**Data Availability Statement:** All datasets generated in this study are available from the corresponding author upon reasonable request.

**Conflicts of Interest:** The authors declare no conflict of interest.

## References

1. Qamaruddin, M.; Chandra, B. Behaviour of Unreinforced Masonry Buildings Subjected to Earthquakes. *Prof. J. Mason. Soc. USA* **1991**, *9*, 47–55.
2. Calvi, G.M.; Pavese, A. Application of Dynamic Identification Techniques to a Brick Masonry Building Prototype. In Proceedings of the 10th European Conference on Earthquake Engineering 1995, Vienna, Austria, 28 August–2 September 1995; pp. 2413–2418.
3. Tomazevic, M. Seismic Upgrading of Old Brick-Masonry Urban Houses: Tying of Walls with Steel Ties. *Earthq. Spectra* **1996**, *12*, 599–622. [[CrossRef](#)]
4. Costley, A.C.; Abrams, S.P. *Dynamic Response of Unreinforced Masonry Buildings with Flexible Diaphragm*; Technical Report No. MCEER-96-0001; MCEER: Washington, DC, USA, 1996.
5. Benedetti, D.; Carydis, P.; Pezzoli, P. Shaking Table Test on 24 Masonry Buildings. *Earthq. Eng. Struct. Dyn.* **1998**, *27*, 67–90. [[CrossRef](#)]
6. Yi, T.; Moon, F.L.; Leon, R.T.; Kahn, L.F. Lateral Load Tests on a Two-story Unreinforced Masonry Building. *ASCE J. Struct. Eng.* **2006**, *132*, 643–652. [[CrossRef](#)]
7. Architectural Institute of Japan (AIJ). *Report on the Damage Investigation of the 1999 Chi-Chi Earthquake*; AIJ: Tokyo, Japan, 2000.
8. Architectural Institute of Japan (AIJ). *Report on the Damage Investigation of the 2006 Central Java Earthquake*; AIJ: Tokyo, Japan, 2007.
9. Manafpour, A.R. Bam Earthquake, Iran: Lessons on the Seismic Behavior of Building Structures. In Proceedings of the 14th World Conference on Earthquake Engineering, Beijing, China, 12–17 October 2008.
10. Sanada, Y.; Kishimoto, I.; Kuroki, M.; Sakashita, M.; Choi, H.; Tani, M.; Hosono, Y.; Fauzan, M.S.; Farida, F. Preliminary Report on Damage to Buildings due to the September 2 and 30, 2009 Earthquakes in Indonesia. In Proceedings of the Eleventh Taiwan-Korea-Japan Joint Seminar on Earthquake Engineering for Building Structures, Kyoto, Japan, 2–3 November 2009; pp. 297–306.
11. Choi, H.; Sanada, Y.; Kuroki, M.; Sakashita, M.; Tani, M.; Hosono, Y.; Musalamah, S.; Farida, F. Comparing Damage to Building Structures Due to the 2009 West Java Earthquake in Indonesia. In Proceedings of the 2nd International Conference on Earthquake Engineering and Disaster Mitigation, Surabaya, Indonesia, 19–20 July 2011.
12. Architectural Institute of Japan (AIJ). *Reconnaissance Report on the 2015 Nepal Gorkha Earthquake*; Architectural Institute of Japan (AIJ): Tokyo, Japan, 2016.
13. Abrams, D.P.; Shah, N. *Cyclic Load Testing of Unreinforced Masonry Walls*; Advanced Construction Technology Centre Report No. 92-26-10; University of Illinois at Urbana Champaign: Champaign, IL, USA, 1992; p. 2.
14. Magenes, G.; Calvi, G.M. Shaking Table Tests on Brick Masonry Walls. In Proceedings of the 10th European Conference on Earthquake Engineering 1995, Vienna, Austria, 28 August–2 September 1995; pp. 2419–2424.

15. Doherty, K.T. An Investigation of the Weak Links in the Seismic Load Path of Unreinforced Masonry Buildings. Ph.D. Thesis, Faculty of Engineering, University of Adelaide, Adelaide, Australia, 2000.
16. Griffith, M.C.; Vaculik, J.; Lam, T.K.; Wilson, J.; Lumtarna, E. Cyclic Testing of Unreinforced Walls in Two-way Bending. *Earthq. Eng. Struct. Dyn.* **2006**, *36*, 801–821. [[CrossRef](#)]
17. Simsir, C.; Aschheim, M.; Abrams, D. Influence of Diaphragm Flexibility on the Out-of-plane Response of Unreinforced Masonry Bearing Walls. In Proceedings of the 9th North American Masonry Conference 2002, Clemson, SC, USA, 28 February 2002.
18. Tomazevic, M. Dynamic Modelling of Masonry Buildings: Storey Mechanism as a Simple Alternative. *Earthq. Eng. Struct. Dyn.* **1987**, *15*, 731–749. [[CrossRef](#)]
19. Moon, K.L. Seismic Strengthening of Low-Rise Unreinforced Masonry Structures with Flexible Diaphragms. Ph.D. Thesis, Georgia Institute of Technology, Atlanta, GA, USA, 2004.
20. Moon, F.L.; Yi, T.; Leon, R.T.; Kahn, L.F. Testing of a Full-Scale Unreinforced Masonry Building Following Seismic Strengthening. *J. Struct. Eng.* **2007**, *133*, 1215–1226. [[CrossRef](#)]
21. Kang, S.H.; Hong, S.G.; Lee, S.J. Rocking Capacity of Unreinforced Masonry Walls. *J. Archit. Inst. Korea-Struct.* **2010**, *26*, 45–56.
22. Yi, W.H.; Lee, J.H.; Oh, S.H.; Yang, W.J.; Kang, D.E. A Study of Evaluation of Shear Capacity of Unreinforced Masonry Wall. *J. Archit. Inst. Korea-Struct.* **2005**, *21*, 3–10.
23. Korea Infrastructure Safety Corporation. *Guidelines for Seismic Performance Evaluation for Existing Buildings*; Korea Infrastructure Safety Corporation: Seoul, Republic of Korea, 2013.
24. American Society of Civil Engineers. *ASCE 41-13 Seismic Evaluation and Retrofit of Existing Buildings*; American Society of Civil Engineers: Reston, VA, USA, 2013.
25. American Society of Civil Engineers. *ASCE 41-17 Seismic Evaluation and Retrofit of Existing Buildings*; American Society of Civil Engineers: Reston, VA, USA, 2017.
26. Esposito, R.; Ravenhorst, G. *Quasi-Static Cyclic In-Plane Tests on Masonry Components*; Delft University of Technology: Delft, The Netherlands, 2017.
27. Mahmoudi Motlagh, S. Numerical Modeling of the In-Plane Seismic Behavior of unreinforced Masonry Wall Retrofitted with Bed Joint Reinforcements. Master's Thesis, Delft University of Technology, Delft, The Netherlands, 2020.
28. Shabani, A.; Kioumarsi, M. A Novel Macroelement for Seismic Analysis of Unreinforced Masonry Buildings Based on MVLEM in OpenSees. *J. Build. Eng.* **2022**, *49*, 104019. [[CrossRef](#)]
29. Eom, T.S.; Kim, C.H.; Lee, S.J.; Kim, J.W. Case Study of Seismic Evaluation of Low-Rise Masonry Buildings. *EESK J. Earthq. Eng.* **2022**, *26*, 1–11.
30. Faulay, T.; Priestly, M.J.N. *Seismic Design of Reinforced Concrete and Masonry Buildings*; John Wiley & Sons: New York, NY, USA, 1992.
31. Xu, W.; Abrams, D.P. Evaluation of Lateral Strength and Deflection for Cracked Unreinforced Masonry Walls. Rep. No. 92-26-11; Advanced Construction Technology Center, College of Engineering, University of Illinois: Urbana, IL, USA, 1992.

**Disclaimer/Publisher's Note:** The statements, opinions and data contained in all publications are solely those of the individual author(s) and contributor(s) and not of MDPI and/or the editor(s). MDPI and/or the editor(s) disclaim responsibility for any injury to people or property resulting from any ideas, methods, instructions or products referred to in the content.